Published by
NIGERIAN SOCIETY OF PHYSICAL SCIENCES
Available online @ https://asr.nsps.org.ng/index.php/asr

African Scientific Reports 5 (2026) 567

African Scientific Reports

Electrochemical performance of hydrothermally synthesized Co-doped NiO electrodes: effect of propylene carbonate additive and doping concentration

Uba Nwankwo[a,b,*], Raphael Mmaduka Obodo[c], Precious Nkechinyere Kalu[a], Chinedum Obed Dike[a], John Elom Ekpe[a], John Ubi Arikpo[a], Kasi Ramesh[b], Subramaniam Ramesh[b], Fabian Ifeanyichukwu Ezema[d]

[a]*Department of Physics, Alex Ekwueme Federal University, Ndufu-Alike, Nigeria*
[b]*Centre for Ionics Universiti Malaya, Department of Physics, Faculty of Science, Universiti Malaya, 50603 Kuala Lumpur, Malaysia*
[c]*Department of Physics, Federal University of Technology, Owerri, Imo State, Nigeria*
[d]*Department of Physics and Astronomy, University of Nigeria, Nsukka, Nigeria*

Abstract

Transition metal oxides have received substantial attention because of their versatile applications in photocatalysis, electronics, and energy storage systems such as batteries and pseudocapacitors. Owing to their variable oxidation states, they are known as redox-active materials, which give rise to battery-type and pseudocapacitor-type electrodes for energy storage devices. In this work, 10%, 20%, and 30% cobalt-doped nickel oxide and 30% cobalt-doped nickel oxide mixed with propylene carbonate (PC) were synthesized via the hydrothermal method to produce electrode materials for a supercapacitor. The electrode materials were characterized by X-ray diffraction (XRD), Fourier transform infrared spectroscopy (FTIR), field-emission scanning electron microscopy–energy-dispersive X-ray spectroscopy (FESEM–EDX), and Brunauer–Emmett–Teller (BET) analyses. The obtained XRD and EDX spectra confirmed crystallinity and elemental composition. The BET surface area of 30% cobalt-doped nickel oxide mixed with PC was estimated to be 17.67 $m^2\ g^{-1}$, which is larger than that of 30% cobalt-doped nickel oxide, with a surface area of 11.05 $m^2\ g^{-1}$. The electrode fabricated with 30% cobalt-doped nickel oxide showed better performance, and its electrochemical performance was further enhanced with the PC additive. The specific capacitance of the 30% cobalt-doped nickel oxide with PC additive reached 551 F g^{-1} at 0.1 A g^{-1} and 661 F g^{-1} at 5 mV s^{-1}. The obtained results suggest that new-generation electrochemical electrodes can be optimized by adding PC during synthesis.

DOI: 10.46481/asr.2026.5.3.567

Keywords: Transition metal oxide, Electrode material, Hydrothermal method, Supercapacitor, Propylene carbonate

Article history:
Received: 02 June 2026
Received in revised form: 20 August 2026
Accepted for publication: 10 September 2026
Available online: 02 October 2026

© 2026 The Author(s). Published by the Nigerian Society of Physical Sciences under the terms of the Creative Commons Attribution 4.0 International license. Further distribution of this work must maintain attribution to the author(s) and the published article's title, journal citation, and DOI.

1. Introduction

In today's smart electronic devices, electrochemical energy storage (EES) devices are indispensable. Technological development is necessary to enhance the characteristics of energy storage devices as global energy demands rise and the need for alternative

*Corresponding Author Tel. No.: +234-810-878-1280.
Email address: nwankwo.uba@funai.edu.ng (Uba Nwankwo)

energy sources grows [1]. Currently, research is ongoing around the globe to improve the performance of energy storage devices in order to satisfy the rising demand for effective and sustainable energy storage systems [2, 3]. Despite these considerable efforts, the development and fabrication of efficient, durable, and high-performance electrodes for energy storage devices remain major challenges.

EES is primarily classified into batteries and electrochemical capacitors (supercapacitors). Supercapacitors are storage devices with high power density, fast charging and discharging, and high cyclic stability. Electric double-layer capacitors (EDLCs), pseudocapacitors, and hybrid capacitors are types of supercapacitors. The type of supercapacitor is mainly determined by the storage mechanism involved. The electrode, separator, and electrolyte are the fundamental components of an EES device [4]. In an EES device with liquid electrolyte, two electrodes are filled with electrolyte, and a separator is placed between the electrodes. However, electrodes play a greater role because they determine the storage mechanism possessed by energy storage devices. Storage mechanisms are described by whether the electrodes are faradaic, involving a reversible reduction–oxidation (redox) reaction, or non-faradaic, which is capacitive and non-reversible. The type of material used for electrode fabrication determines the storage mechanism. Carbon-based materials exhibit a capacitive storage mechanism, while transition metal oxides (TMOs) and conducting polymers are electrode materials that exhibit a faradaic storage mechanism. In capacitive-type or EDLC electrodes, ion adsorption occurs, whereas in faradaic-type (battery-type or pseudocapacitor-type) electrodes, a redox reaction occurs at the interface between the electrodes and the electrolyte [5, 6].

TMO electrode materials have drawn considerable interest because they can be used as both battery-type and pseudocapacitor-type electrodes. Various TMOs have been employed as battery-type and pseudocapacitor-type materials owing to the multiple oxidation states of transition metals (TMs). The most commonly used transition metals and their oxides are nickel (Ni), titanium (Ti), cobalt (Co), manganese (Mn), and vanadium (V), and nickel oxide (NiO), titanium oxide (TiO_2), cobalt oxide (Co_3O_4), manganese oxide (MnO_2), and vanadium oxide (V_2O_5), respectively. TMOs are environmentally friendly and cheap to synthesize and have high theoretical energy and power densities [7–9]. However, significant challenges have hindered the efficient performance of these electrodes in supercapacitors, such as low electrical conductivity, high equivalent series resistance (ESR), and increased volume during cyclic stability tests. To address these drawbacks, numerous research steps have been carried out on TMO materials.

The effect of a graphene oxide (GO) additive on Co_3O_4 (GO/Co_3O_4) and NiO (GO/NiO) for supercapacitor electrodes has been studied. The electrodes showed specific capacitance values of 1156 F g^{-1} and 775 F g^{-1} at 1 mV s^{-1} [10]. The hydrothermal synthesis of $NiCoO_x$ and $NiCo_2O_x$ for application in photocatalysis, rather than electrochemical applications, was reported [11]. NiO electrode materials synthesized by the green synthesis technique showed 156 F g^{-1}, 183 F g^{-1}, and 85% capacitance retention [12]. Thin films of Mn–Ni–Co oxide/GO coated on copper foam using electrodeposition were studied, and a value of 475 F g^{-1} was obtained [13]. NiCuCo mixed oxide electrode material synthesized by the hydrothermal method showed a specific capacity of 506 C g^{-1} at 1 A g^{-1} alongside 99% capacity retention for 1000 cycles [14]. A freestanding cobalt-doped nickel oxide nanosheet electrode fabricated on carbon-welded carbon nanotube foam was studied to improve supercapacitor performance, and its evaluation showed 11.45 F cm^{-2} at 5 mA cm^{-2} [15]. Despite the numerous reports on TMO-based electrode materials, only a few reports have presented a cheap method of synthesis while maintaining high specific capacitance.

In this work, 10%, 20%, and 30% cobalt-doped nickel oxide and 30% cobalt-doped nickel oxide with propylene carbonate (PC) nanoparticles were synthesized using the hydrothermal method. The electrochemical activities were studied in a three-electrode configuration using the as-synthesized materials as the working electrode. The effect of the PC additive on 30% cobalt-doped nickel oxide was studied. PC is an organic solvent that is biodegradable, cheap, and non-toxic [16]. These results suggest that PC additives can be employed to advance the characteristics of energy-storage devices.

2. Materials and methods

2.1. Materials for synthesis

Nickel(II) chloride hexahydrate ($NiCl_2{\cdot}6H_2O$), cobalt(II) nitrate hexahydrate ($Co(NO_3)_2{\cdot}6H_2O$), PC, sodium hydroxide (NaOH), N-methyl-2-pyrrolidone (NMP), hydrochloric acid (HCl), potassium hydroxide (KOH), acetone, and polyvinylidene difluoride (PVDF) were purchased from chemical stores. Carbon black and Ni foam were purchased from China. The electrode materials were prepared using the hydrothermal synthesis method.

2.2. Experimental methods

Cobalt-doped nickel oxide electrode materials were synthesized using the hydrothermal method. $Co(NO_3)_2{\cdot}6H_2O$ (4.4 g) in 60 mL of distilled water and nickel(II) chloride hexahydrate ($NiCl_2{\cdot}6H_2O$; 11.89 g) in 200 mL of distilled water were used as the Co and Ni sources, respectively, while the concentrations of both precursor solutions were kept at 0.25 M. The Ni and Co precursor solutions were stirred in separate beakers at room temperature for 1 h for the salts to dissolve. NaOH (2.0 g) was dissolved in 50 mL of distilled water, and 5 mL of NaOH (1 M) was added to the Ni–Co precursor solution to obtain pH 7. Before adjustment of the solution pH, 10 vol%, 20 vol%, and 30 vol% of 60 mL of the Co precursor solution were added to beakers containing 60 mL of Ni precursor solution and labelled beakers 1, 2, and 3. The mixture of the two precursor baths was stirred for 0.75 h at 27 °C before being transferred to

Table 1: The synthesized electrode materials and their acronyms.

Synthesized material	Acronym
10% Co-doped NiO	10% CN
20% Co-doped NiO	20% CN
30% Co-doped NiO	30% CN
30% Co-doped NiO + PC	30% CN+PC

three separate 100 mL Teflon-lined stainless-steel autoclaves. The same process was repeated for the 30% volume of Co precursor and 60 mL of Ni precursor with 0.01 mL of the organic solvent (PC) in the bath. The autoclaves were preheated at 150 °C for 18 h. The obtained solution was cleaned using distilled water and ethanol to remove impurities and then dried overnight at 60 °C. The resulting nanoparticles were calcined at 550 °C for 3 h to obtain 10% CN, 20% CN, 30% CN, and 30% CN+PC. The full meanings of the acronyms are provided in Table 1.

3. Material characterization

3.1. Structural characterization

The 30% CN and 30% CN+PC electrode materials were evaluated using an X-ray diffractometer (XRD; Rigaku SmartLab diffractometer) with a theta–theta goniometer and CuKα radiation ($\lambda \sim 0.154$ nm), with 2θ ranging from 20° to 80°. Morphology and elemental mapping were performed at room temperature using FEI Quanta FEG 450 field-emission scanning electron microscopy (FESEM). A Thermo Scientific Fourier transform infrared (FTIR) spectrophotometer was used to obtain the fingerprint spectrum between 4000 and 400 cm^{-1}, and a Brunauer–Emmett–Teller (BET) TriStar 3020 Micromeritics instrument was used to measure the surface area of the nanoparticles at 77 K in a nitrogen atmosphere.

3.2. Electrochemical studies

The electron kinetics of the as-synthesized electroactive materials were studied by immersing the coated electroactive material in 2 M KOH, used as the aqueous electrolyte in a half-cell setup. The Ni foam used in this study was washed in 0.5 M HCl and distilled water and then cleaned in acetone. Each washing step was subjected to sonication for 20 min, followed by overnight drying at 60 °C. The active materials, carbon black, and PVDF were combined in a percentage ratio of 80:10:10, respectively, to form a fine slurry. The slurry was deposited with a paint brush on an area of 1 cm × 1 cm on the Ni foam and dried for 15 h at 50 °C. The coated electroactive materials were used as working electrodes (10% CN, 20% CN, 30% CN, and 30% CN+PC), while Ag/AgCl was the reference electrode and platinum wire was the counter electrode. The mass loading was measured by taking the difference between the bare mass of the Ni foam and the coated Ni foam. The mass loading per square centimeter was maintained between 2.2 and 2.6 mg cm^{-2}.

4. Results and discussion

4.1. Structural examination

4.1.1. XRD evaluations

The XRD patterns of 30% CN and 30% CN with PC additive are shown in Figure 1. The XRD patterns for 30% CN and 30% CN with PC additive correspond to the XRD spectra of the host material (NiO). The observed 2θ peaks at 31°, 36.90°, 42.60°, 62.50°, 73.80°, and 79° correspond to the (110), (111), (200), (220), (311), and (222) crystal phases of face-centered cubic NiO, corresponding to JCPDS No. 04-0835. However, the peaks appearing around 2θ = 19°, 58°, and 65° correspond to Co_3O_4 (JCPDS No. 73-2181). In contrast to the XRD peaks observed for NiO and Co_3O_4, the additional peaks appearing in the XRD spectra of 30% CN with PC additive can be attributed to the presence of the PC additive. The XRD spectra show that both electrode materials exhibit a high degree of crystallinity.

4.1.2. The FTIR evaluation

Figure 2 depicts the FTIR spectra of 30% CN and 30% CN+PC nanoparticles. The functional groups identified in the FTIR measurement correspond to the hydroxyl group at 3460 cm^{-1}, the carboxyl group at 1600 cm^{-1}, the carboxylic group between 1100 and 1321 cm^{-1}, and the metal oxide around 450 and 550 cm^{-1}. However, the FTIR spectra of the material with PC additive show a different signature, which is the effect of the PC additive on the material during synthesis.

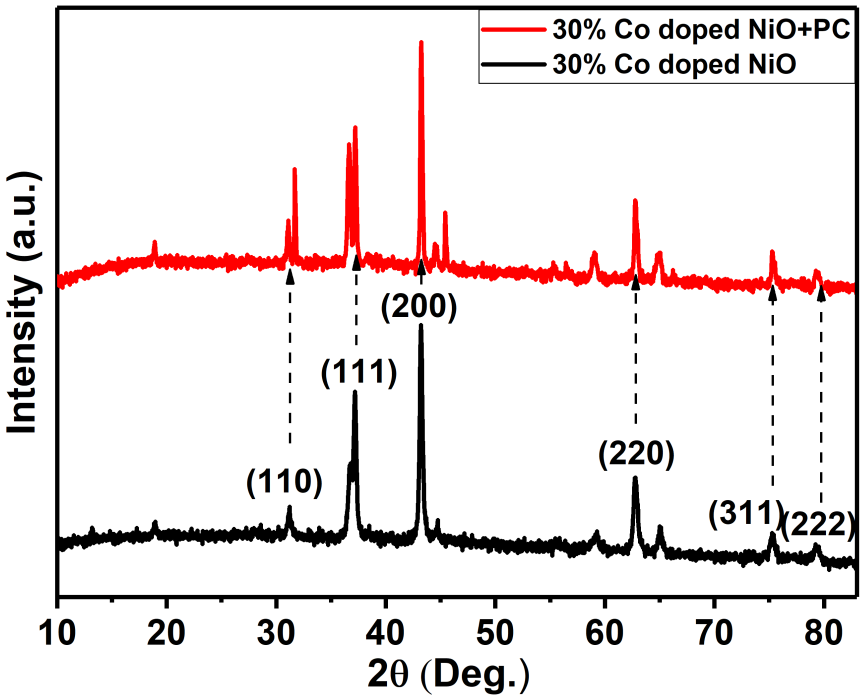

Figure 1: XRD spectra of 30% CN and 30% CN+PC nanoparticles.

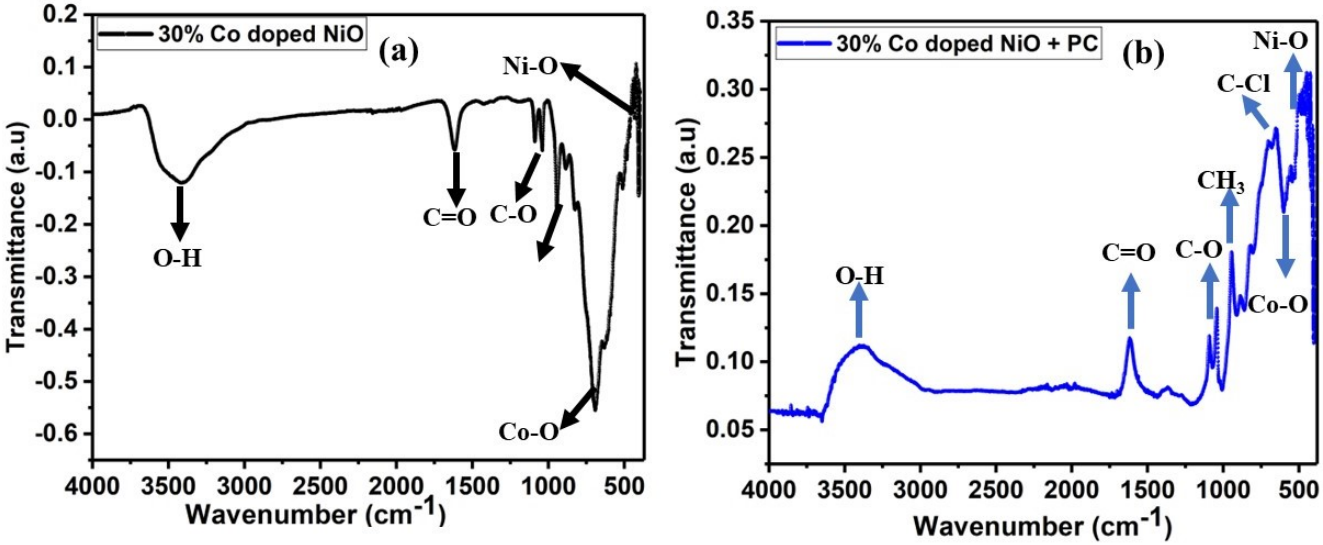

Figure 2: FTIR analysis of (a) 30% CN and (b) 30% CN+PC nanoparticles in the range of 4000–400 cm^{-1}.

4.1.3. The FESEM images and EDX analysis

The FESEM images of the 30% CN and 30% CN+PC nanoparticles are shown in Figure 3. The FESEM image of the material prepared by adding the PC additive shows slight particle aggregation as a result of the interaction between the precursor solvent and the PC solution. The FESEM images of 30% CN and 30% CN+PC show nanoflakes and a regular semi-spherical shape, respectively. The FESEM images reveal distinct modification of the electrode material surface morphology following incorporation of the PC additive during synthesis. The semi-spherical shape observed in the electrode material with PC additive promotes better adhesion of the active material to the nickel foam, thereby improving electron transport and electrochemical performance.

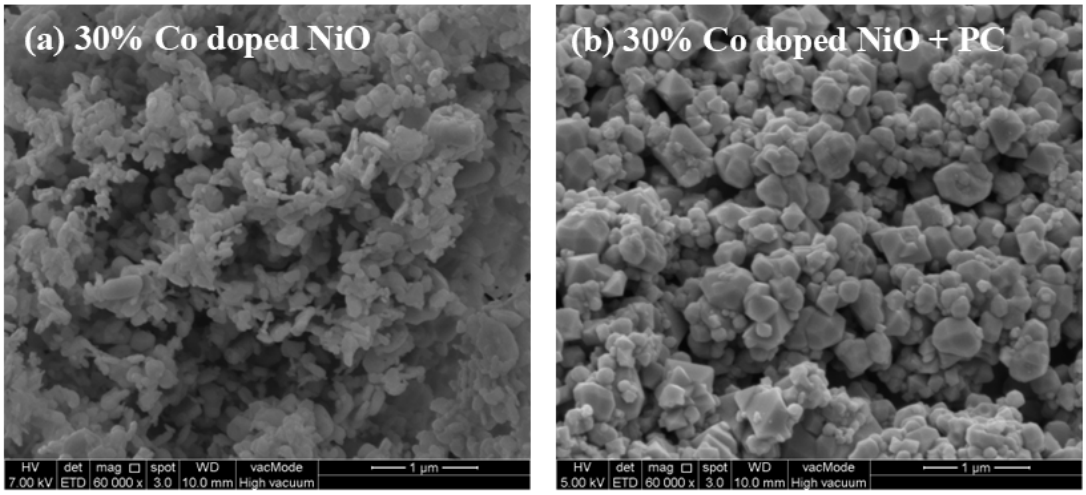

Figure 3: FESEM images of (a) 30% CN and (b) 30% CN+PC nanoparticles.

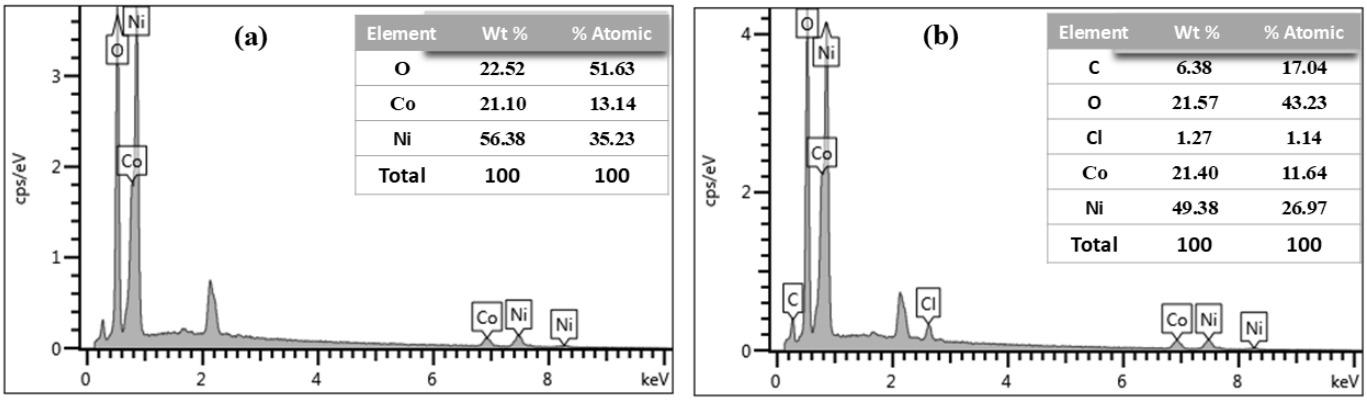

Figure 4: EDX elemental composition of (a) 30% CN and (b) 30% CN+PC nanoparticles.

The elemental compositions of the 30% CN and 30% CN+PC materials were established by EDX analysis. Figure 4 shows the EDX spectra of 30% CN and 30% CN+PC and the elemental distributions of the materials. The atomic and weight percentages of the elemental compositions are presented in the inset of Figure 4. No impurities are present in the EDX results.

4.1.4. BET analyses

The BET measurement results of the 30% CN and 30% CN+PC nanoparticles are presented in this section. The isotherm linear plots for 30% CN and 30% CN+PC nanoparticles are depicted in Figure 5. The linear isotherm plot shows slight hysteresis during the adsorption and desorption procedures. Both exhibit a type IV isotherm, according to IUPAC classifications. The estimated BET surface areas, pore sizes, and pore volumes for the 30% CN and 30% CN+PC nanoparticles are 11.05 $m^2\ g^{-1}$, 39.73 nm, and 0.1096 $cm^3\ g^{-1}$, and 17.67 $m^2\ g^{-1}$, 22.07 nm, and 0.0975 $cm^3\ g^{-1}$, respectively. The pore sizes of the materials fall in the range of 2–50 nm, showing that both nanoparticles are mesoporous. The BET pore-structure parameters exhibited a strong relationship with the electrochemical performance of the electroactive materials. Increased pore size and pore volume promote efficient ion transport during the charging–discharging process. However, sufficiently large pores may impede the effective surface area available for charge storage. The electrode material with PC additive shows a smaller pore size and increased surface area, which provided better electrochemical performance than the electrode material without PC additive.

4.2. Electrochemical analysis

This analysis involved different fabricated electrodes, and the following investigations were carried out: cyclic voltammetry (CV), galvanostatic charge–discharge (GCD), and electrochemical impedance spectroscopy (EIS). The obtained data were used to calculate

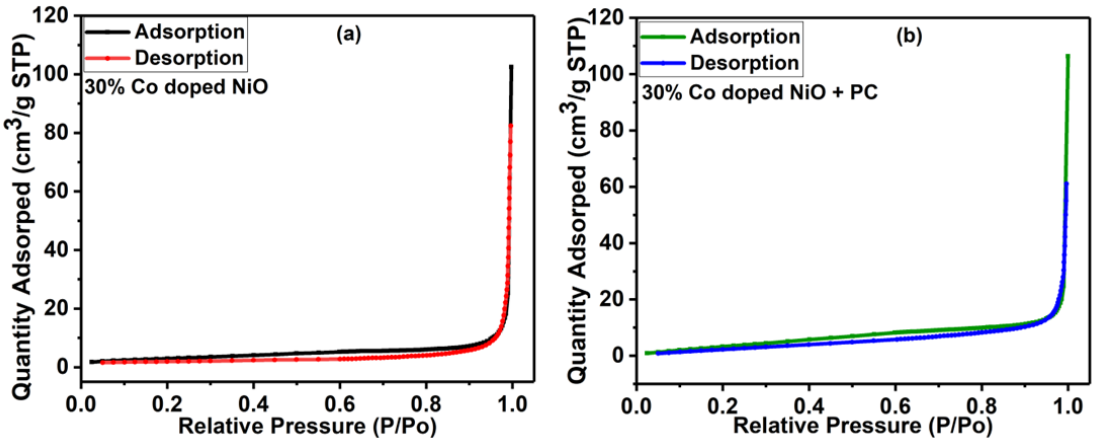

Figure 5: Isotherm linear plot of (a) 30% CN and (b) 30% CN+PC nanoparticles.

the specific capacitance (C_{sp}, F g^{-1}) from CV and GCD using Eq. (1) and Eq. (2), respectively:

$$C_{sp} = \frac{\int i(V)\,\mathrm{d}V}{m\nu\Delta V}, \tag{1}$$

$$C_{sp} = \frac{i \times t_d}{m \times \Delta V}. \tag{2}$$

Here, $\int i(V)\,\mathrm{d}V$ is the absolute area under the CV curves, i is the applied current (A), t_d is the discharge period (s), ΔV is the operating potential window (V), ν is the scan rate (V s^{-1}), and m is the mass loading (g).

4.2.1. Cyclic voltammetry

The CV curves of the 10%, 20%, and 30% CN and 30% CN+PC electrodes were analyzed in the voltage range of 0–0.5 V at 5–50 mV s^{-1}, as shown in Figure 6. The shapes of the CV curves for all the as-synthesized electrode materials show redox peaks, which is evidence of a faradaic reaction at the boundary between the electrodes and the electrolyte. The CV curves for the electrode with PC additive at the anodic peak deviate at the scan rate of 50 mV s^{-1}. The current response of the CV curves increases with the scan rates.

The absolute area under the CV curves shows a maximum value for the electrode with PC additive compared with x% CN (where x = 10, 20, and 30) without PC additive, indicating improved specific capacitance as a result of the incorporation of the organic additive (PC). Figure 7 depicts the C_{sp} of the electrode materials at a scan rate of 5 mV s^{-1}. The highest achieved C_{sp} of 661 F g^{-1} was observed for the 30% CN+PC electrode material. The observed C_{sp} in the electrode materials with PC additive was accompanied by an increase in current response and the absolute area under the CV curve. The well-defined presence of redox peaks for all the as-synthesized electrode materials indicates that they are battery-type electrodes.

The anodic and cathodic redox peaks obtained from the oxidative and reductive scans of the CV curves were used as the peak currents (I_{pa} and I_{pc}) and the corresponding potentials (E_{pa} and E_{pc}), respectively, as demonstrated in Figure 8. Various ratios attained by the anodic peak currents to the cathodic peak currents at a scan rate of 10 mV s^{-1} were calculated for the two samples, 30% CN and 30% CN+PC, with peak-current ratios of 1.1 and 1.08, respectively, against the theoretical value of 1 [17].

To confirm the behavior of the charge-storage mechanisms involved in the CV loop of the two best-performing electrodes, the Tafel plot and Randles–Sevcik equation were used according to Eq. (3) and Eq. (4), respectively:

$$i = a\nu^{b}, \tag{3}$$

$$i_p = a\nu^{1/2}. \tag{4}$$

Here, i is the current, i_p is the peak current, ν is the scan rate, and b is the slope of the plot.

Figure 9 depicts the plots of the peak currents against the square roots of the scan rates and the logarithm of the peak currents against the logarithm of the scan rates. The linear behavior detected in the peak currents against the square roots of the scan rates shows that the charge-storage mechanism involved is a diffusion-controlled process.

The b-values obtained from the plot of Tafel's relation for the two best-performing electrodes are b = 0.47 and 0.53 and b = 0.46 and 0.54 for the anodic and cathodic peaks of 30% CN and 30% CN+PC, respectively. The b-values further confirm that charge storage is a diffusion-controlled process. Therefore, the CV curves and the analysis reveal that the electrode is a battery-type electrode, which is supported by the redox peaks related to the faradaic process.

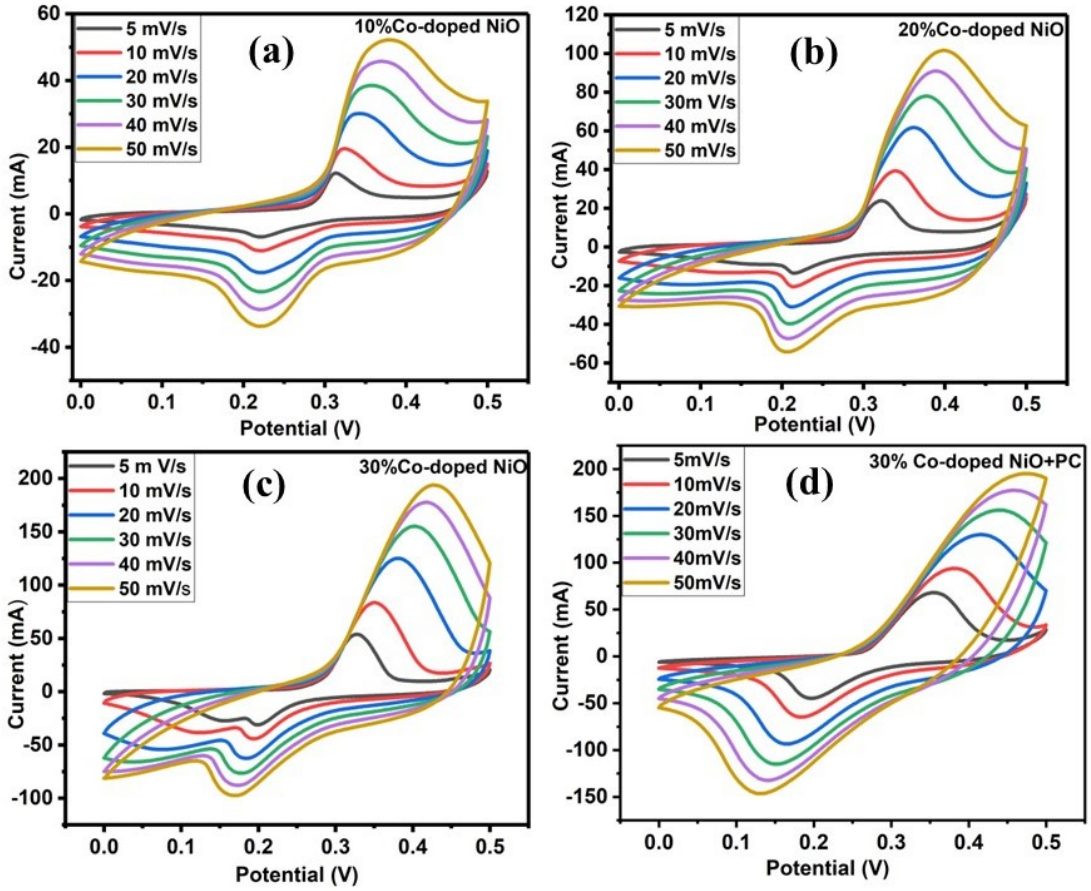

Figure 6: CV curves for various scan rates: (a) 10% CN, (b) 20% CN, (c) 30% CN, and (d) 30% CN+PC.

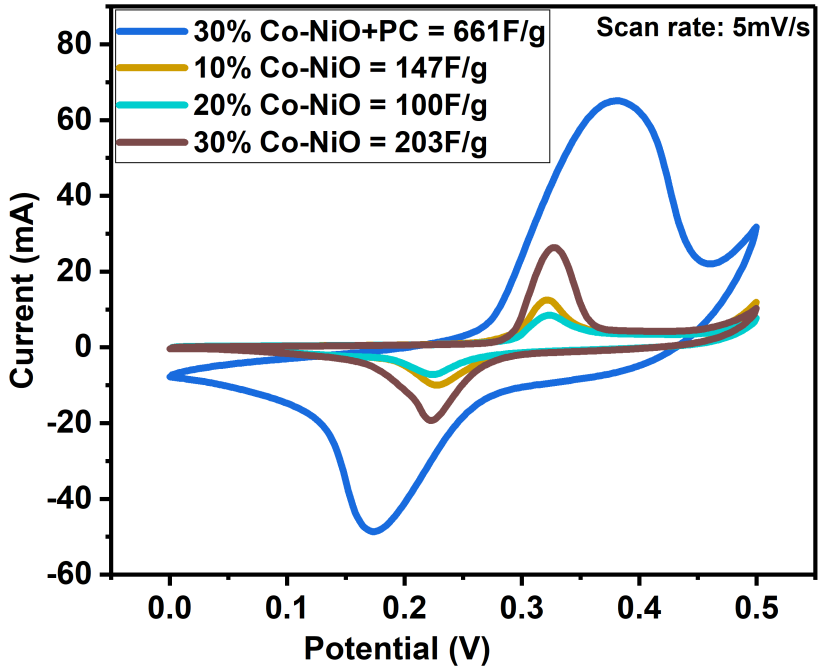

Figure 7: CV curve showing the specific capacitance of 10%, 20%, and 30% CN and 30% CN+PC at a 5 mV s^{-1} scan rate.

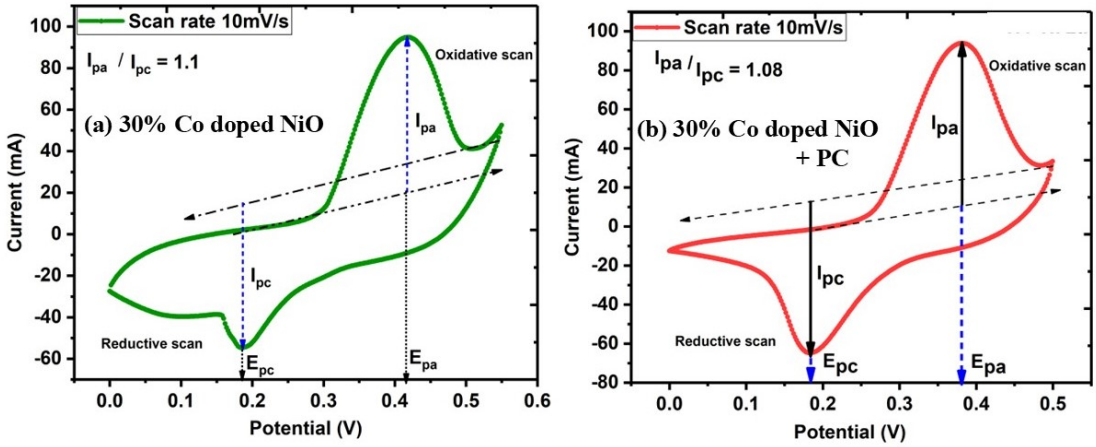

Figure 8: Plot showing the peak current and potential values in the oxidative and reductive scans for (a) 30% CN and (b) 30% CN+PC at a scan rate of 10 mV s^{-1}.

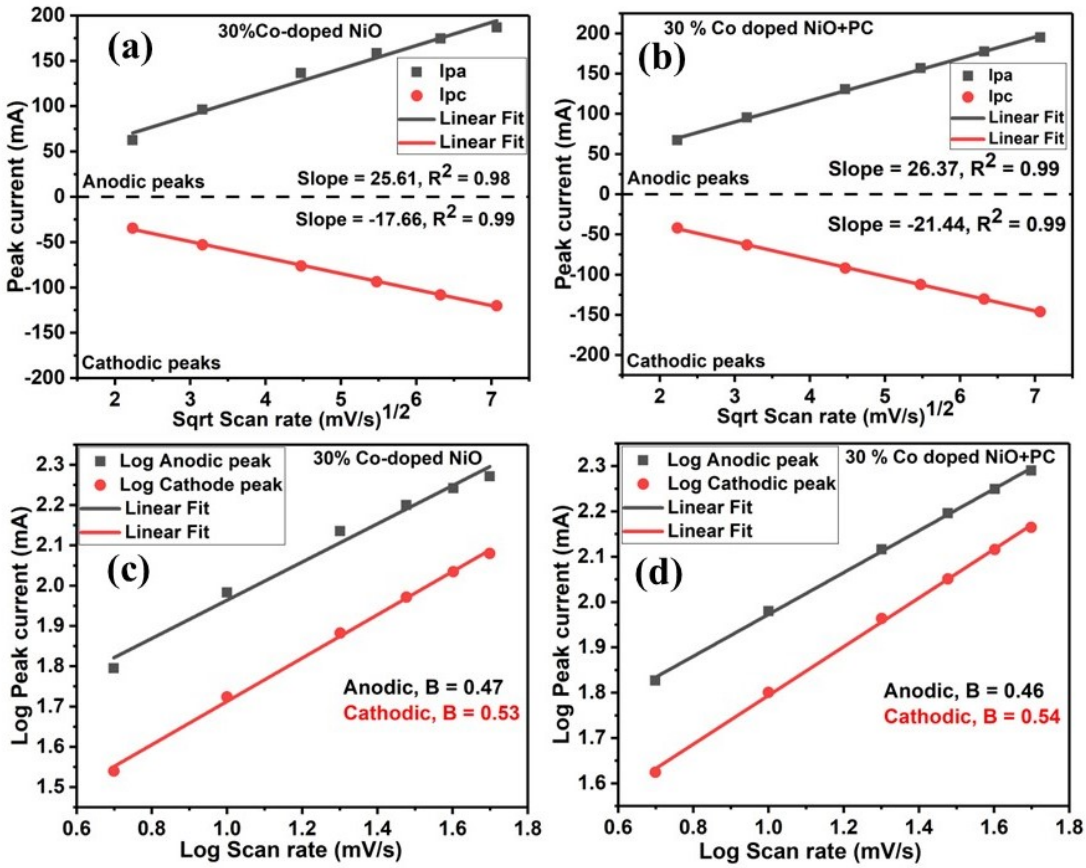

Figure 9: Linear plot of peak currents against the square roots of scan rates and log of peak currents against log of scan rates, showing anodic and cathodic *b*-values for 30% CN and 30% CN+PC.

4.2.2. Galvanostatic charge–discharge analysis

The GCD graphs of the electrodes measured at 0.1 A g^{-1} and 0.5–3.0 A g^{-1} current densities show nonlinear behavior of the potential–time curves, which confirms battery-type behavior of the electrode material, as shown in Figure 10(a,b).

For the electrode materials, there is evidence of a plateau shape in the GCD curve, which is characteristic of battery-type behavior [7]. The maximum specific capacitance calculated using Eq. (2) and the discharge curve of Figure 10(c) at 0.1 A g^{-1} is 226 F g^{-1} and 551 F g^{-1} for 30% CN and 30% CN+PC, respectively. The specific capacitance obtained from the GCD curves decreases as the

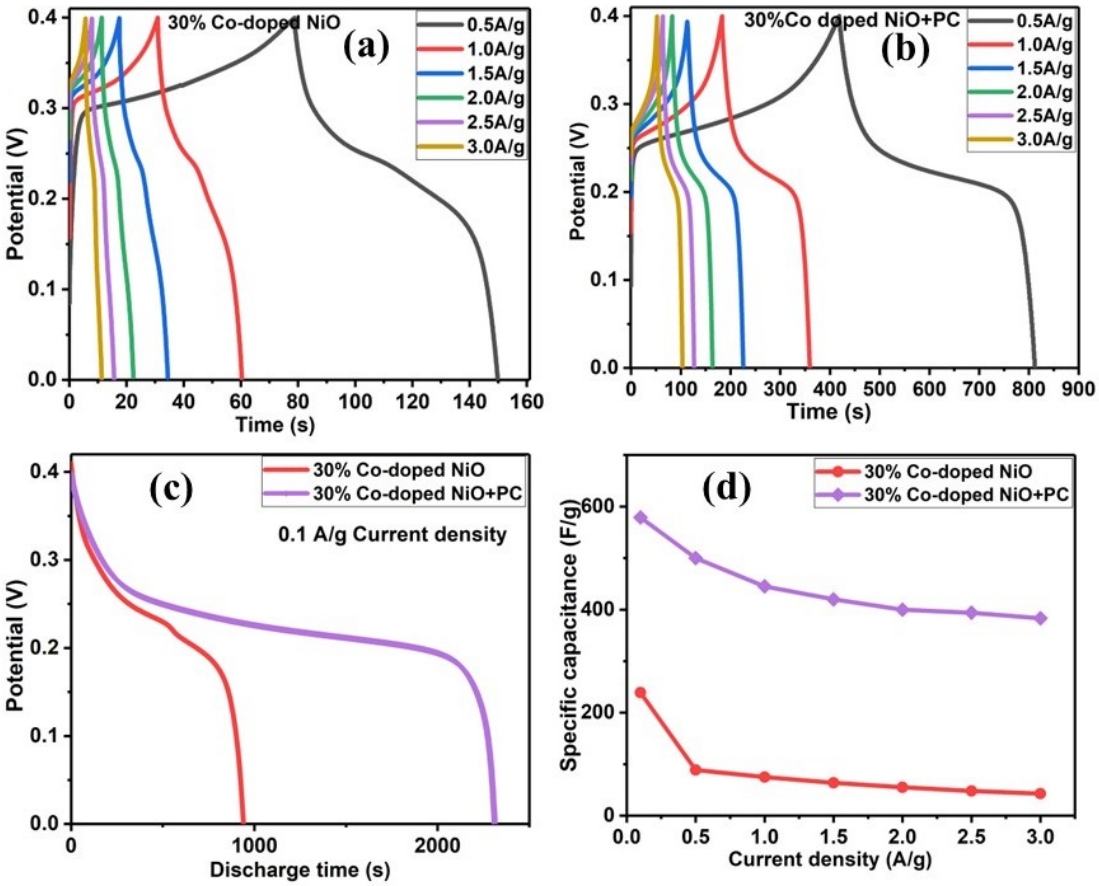

Figure 10: (a,b) GCD curves at various current densities, (c) discharge curve at a current density of 0.1 A g^{-1}, and (d) variation of C_{sp} at various current densities for 30% CN and 30% CN+PC.

Table 2: Comparative electrochemical behavior of selected electrodes.

Electrode material	Electrolyte	Condition	C_{sp}	Synthesis method	Ref.
NiO	1 M KOH	10 mV s^{-1}	128 F g^{-1}	Hydrothermal	[18]
Co-doped NiO	2 M Na_2SO_4	10 mV s^{-1}	555.62 F g^{-1}	Hydrothermal	[19]
MoS_2/MnO_2	0.5 M Na_2SO_4	0.04 A g^{-1}	199.12 F g^{-1}	Hydrothermal	[20]
Mn–Ni–Co oxide/graphene	6 M KOH	5 mV s^{-1}	531 F g^{-1}	Electrodeposition	[13]
V_2O_5	3 M KOH	0.1 A g^{-1}	6.1 F g^{-1}	Hydrothermal	[21]
30% CN	2 M KOH	0.1 A g^{-1} (5 mV s^{-1})	203 (226) F g^{-1}	Hydrothermal	This work
30% CN+PC	2 M KOH	0.1 A g^{-1} (5 mV s^{-1})	661 (551) F g^{-1}	Hydrothermal	This work

current density increases, as shown in Figure 10(d).

The comparative electrochemical performance of some selected transition metal oxides and transition-metal-doped oxides is presented in Table 2.

4.2.3. The EIS evaluation

The EIS spectra of the 10%, 20%, and 30% CN and 30% CN+PC electrodes are presented as Nyquist plots in Figure 11. The EIS measurement was conducted in the frequency range of 10 mHz to 100 kHz, corresponding to low- and high-frequency regions at a 10 mV AC signal. The EIS spectra give information about impedance parameters, such as electrolyte resistance (R_E), charge-transfer resistance (R_{CT}), Warburg diffusion resistance (W), and the constant phase element (Q_{CE}) of the double-layer capacitance.

The semicircle in the Nyquist plot is observed in the high-frequency region, and the straight line is observed in the low-frequency region. The semicircle length was used to estimate charge-transfer resistance, while the gradient of the straight line and the intercept on the real axis of the impedance give information about Warburg resistance and electrolyte resistance, respectively. The EIS fitted results in Table 3 show that the electrodes with organic additive (PC) have a lower R_{CT} value than the electrodes without PC, indicating

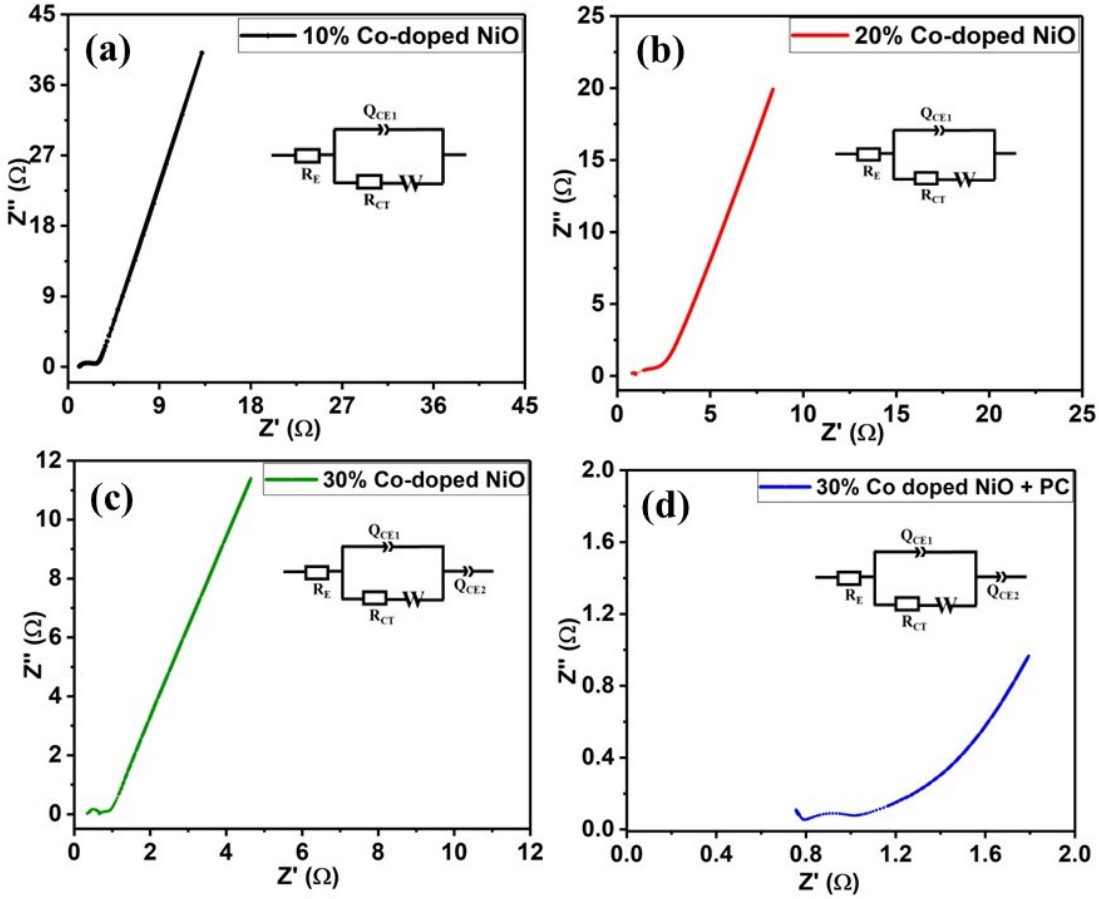

Figure 11: EIS plots (inset: equivalent circuit illustration) of (a) 10% CN, (b) 20% CN, (c) 30% CN, and (d) 30% CN+PC.

Table 3: EIS fitted parameters extrapolated from the Nyquist plot.

Electrode material	R_E (Ω)	R_{CT} (Ω)
10% CN	0.58	0.95
20% CN	1.06	2.07
30% CN	0.58	1.43
30% CN+PC	0.59	0.23

better ionic diffusion at the interface between the electrolyte and electrodes. However, the real and imaginary resistances decrease as the doping level increases, as shown in Figure 11.

5. Conclusion

We successfully synthesized 10%, 20%, and 30% cobalt-doped nickel oxide and 30% cobalt-doped nickel oxide + PC supercapacitor electrode materials using the hydrothermal method. The effects of the PC additive on the structural and electrochemical properties were studied. The XRD and EDX spectra confirmed the crystalline nature and elemental composition of the synthesized electrode materials. The FESEM images show nanoflakes and discrete-shape nanoparticles for 30% CN and 30% CN+PC, respectively. The BET surface areas were estimated as 11.05 and 17.67 $m^2\ g^{-1}$ for 30% CN and 30% CN+PC, respectively. The 30% CN and 30% CN+PC electrode materials display specific capacitance of (226 and 203 F g^{-1}) and (551 and 661 F g^{-1}) at a current density of 0.1 A g^{-1} and scan rate of 5 mV s^{-1}, respectively. The EIS results revealed that the 30% CN+PC electrode exhibited the lowest charge-transfer resistance among the investigated electrode materials. The electrochemical studies reveal that both electrode materials behave like battery-type electrodes. This study shows that the electrochemical properties of transition metal oxide electrodes can be enhanced by incorporating PC additive during material synthesis.

Data availability

The data that support the findings of this study will be made available by the corresponding author upon request.

Declaration of competing interest

The authors declare that they have no known competing financial interests or personal relationships that could have appeared to influence the work reported in this manuscript.

Funding

This work received financial support from AEFUNAI TETFUND under grant number TETF/DASTD/EBONYI/TSAS/2024.

Acknowledgment

The authors appreciate the technical and financial support of Lab. 420, Universiti Malaya, Malaysia, and AEFUNAI TETFUND under grant number TETF/DASTD/EBONYI/TSAS/2024.

References

[1] S. Sharma & P. Chand, "Supercapacitor and electrochemical techniques: a brief review", Results in Chemistry **5** (2023) 100885. https://link.springer.com/article/10.1007/s10904-025-03861-x.

[2] A. Soam, R. Kumar, B. K. Singh & D. S. Saini, "A comprehensive review on synthesis of nanocomposites for supercapacitor", Journal of Inorganic and Organometallic Polymers and Materials **35** (2025) 9619. https://doi.org/10.1007/s10904-025-03861-x.

[3] A. T. Admase, E. D. Asrade & S. W. Fanta, "A comprehensive review on energy storage materials & technologies: applications of nanofabrication techniques for enhanced performance and efficiency", Materials for Renewable and Sustainable Energy **14** (2025) 56. https://doi.org/10.1007/s40243-025-00329-3.

[4] U. Ulissi & R. Raccichini, "Past, present, and future of electrochemical energy storage: a brief perspective", Frontiers of Nanoscience **19** (2021) 1. https://doi.org/10.1016/B978-0-12-821434-3.00013-2.

[5] G. Z. Chen, "Linear and non-linear pseudocapacitances with or without diffusion control", Progress in Natural Science: Materials International **31** (2021) 792. https://doi.org/10.1016/j.pnsc.2021.10.011.

[6] S. Payá, M. D. Casal, N. Díez & M. Sevilla, "A single route for the production of battery-type and capacitor-type electrode materials", Carbon **235** (2025) 120056. https://doi.org/10.1016/j.carbon.2025.120056.

[7] B. Raut, M. Ahmed, H. Kim, M. K. Rahman, G. Bao, M. Islam & K. Nam, "Battery-type transition metal oxides in hybrid supercapacitors: synthesis and applications", Batteries **11** (2025) 60. https://doi.org/10.3390/batteries11020060.

[8] B. Guo, Y. Gao, Y. Li, K. Liu, X. Lv, C. Mi, L. Liu & M. Li, "Battery-type-behavior-retention $Ni(OH)_2$–rGO composite for an ultrahigh-specific-capacity asymmetric electrochemical capacitor electrode", ACS Omega **8** (2023) 6289. https://doi.org/10.1021/acsomega.2c06207.

[9] F. Yu, T. Huang, P. Zhang, Y. Tao, F. Cui, Q. Xie, S. Yao & F. Wang, "Design and synthesis of electrode materials with both battery-type and capacitive charge storage", Energy Storage Materials **22** (2019) 235. https://doi.org/10.1016/j.ensm.2019.07.023.

[10] R. M. Obodo, S. Mbam, H. Nsude, M. Ramzan, S. Ezike, I. Ahmad, M. Maaza & F. Ezema, "Graphene oxide enhanced Co_3O_4/NiO composite electrodes for supercapacitive devices applications", Applied Surface Science Advances **9** (2022) 100254. https://doi.org/10.1016/j.apsadv.2022.100254.

[11] F. Sultan, J. Zhu, D. I. Medina, P. P. Pescarmona, J. L. Cholula-Díaz & D. M. Morales, "Nickel cobalt oxide-based heterostructures as electrocatalysts for the oxygen evolution reaction at industry-relevant conditions", International Journal of Hydrogen Energy **114** (2025) 440. https://doi.org/10.1016/j.ijhydene.2025.02.449.

[12] N. Ahamed, J. Pattar, R. Murthy, M. Kumar, V. Bhoomika, N. Raghavendra & C. Ravikumar, "Electrochemical studies of nickel oxide nanoparticles via solution combustion method using green and chemical fuels", Sustainable Chemistry for the Environment **5** (2024) 100063. https://doi.org/10.1016/j.scenv.2024.100063.

[13] K. Lee, G. Pan, T. Yang, P. Shen, K. Pan, T. Tiong, A. Nikoloski & C. Huang, "Hierarchical manganese-doped nickel–cobalt oxide electrodes with graphene for use as high-energy-density supercapacitors", Surfaces **8** (2025) 43. https://doi.org/10.3390/surfaces8030043.

[14] M. Manikandan, E. Manikandan, V. Swetha, S. Kurpaa, S. Vijay & V. Kiruthika, "Nickel-copper-cobalt mixed oxide electrode material for high performance asymmetric supercapacitor", Scientific Reports **14** (2024) 10821. https://doi.org/10.1038/s41598-024-61625-y.

[15] H. Xu, Y. Cao, Y. Li, P. Cao, D. Liu, Y. Zhang & Q. Li, "High-loading Co-doped NiO nanosheets on carbon-welded carbon nanotube framework enabling rapid charge kinetic for enhanced supercapacitor performance", Journal of Energy Chemistry **50** (2020) 240. https://doi.org/10.1016/j.jechem.2020.03.023.

[16] T. K. S. Fayaz, H. K. Chanduluru, R. H. Obaydo & P. Sanphui, "Propylene carbonate as an ecofriendly solvent: stability studies of ripretinib in RPHPLC and sustainable evaluation using advanced tools", Sustainable Chemistry and Pharmacy **37** (2024) 101355. https://doi.org/10.1016/j.scp.2023.101355.

[17] M. Rafiee, D. J. Abrams, L. Cardinale, Z. Goss, A. Romero-Arenas & S. S. Stahl, "Cyclic voltammetry and chronoamperometry: mechanistic tools for organic electrosynthesis", Chemical Society Reviews **53** (2024) 566. https://doi.org/10.1039/d2cs00706a.

[18] D. P. Mali, R. T. Patil, A. S. Patil & V. J. Fulari, "Facile synthesis of NiO nanoflakes via hydrothermal route: effect of urea concentration", Chemical Physics Letters **770** (2021) 138431. https://doi.org/10.1016/j.cplett.2021.138431.

[19] N. A. Mala, M. A. Dar, S. Sivakumar, K. S. Bhat, G. N. Sinha & K. M. Batoo, "Electrochemical supremacy of cobalt-doped nickel oxide and its supercapacitor applications with its mesoporous morphology", Journal of Materials Science: Materials in Electronics **33** (2022) 11582. https://doi.org/10.1007/s10854-022-08130-y.

[20] M. R. Islam, M. Rahaman, M. M. Billah & M. R. Islam, "Hydrothermal synthesis of an MoS_2/MnO_2 nanocomposite: a unique 3D-nanoflower/1D-nanorod structure for high-performance energy storage applications", Materials Advances **5** (2024) 5307. https://doi.org/10.1039/d4ma00065j.

[21] A. Temam, S. Getaneh, A. Alshoaibi, C. Awada, A. Nwanya, F. Ezema & P. Ejikeme, "Effect of synthesis method on electrochemical activities of V_2O_5 nanoparticles for supercapacitor application", Journal of Materials Science: Materials in Electronics **36** (2025) 763. https://doi.org/10.1007/s10854-025-14816-w.